Agricultural Water Management 241 (2020) 106366

Contents lists available at ScienceDirect

Agricultural Water Management

journal homepage: www.elsevier.com/locate/agwat

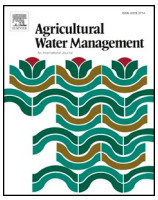

Sensitivity of hydrology and water quality to variation in land use and land cover data

Avay Risal[a], Prem B. Parajuli[a,*], Padmanava Dash[b], Ying Ouyang[c], Anna Linhoss[a]

[a] Department of Agricultural and Biological Engineering, Mississippi State University, Mississippi State, MS, 39762, USA
[b] Department of Geosciences, Mississippi State University, Mississippi State, MS, 39762, USA
[c] Center for Bottomland Hardwoods Research, USDA Forest Service, Mississippi State, MS, 39762, USA

ARTICLE INFO

Keywords:
LULC
Seasonal variation
Hydrology
Water quality
SWAT

ABSTRACT

Land use and land cover (LULC) change is critical to hydrologic study as it affects surface runoff, sediment yield, and nutrient load from watersheds. Change in LULC is a continuous process in agricultural watersheds as per the growing and harvesting seasons. In this study, monthly LULC data layers were generated for the Big Sunflower River Watershed (BSRW), Mississippi by classifying cloud free Landsat images from 2014 to 2018 and combining them according to the season in order to obtain dominant LULC data layers for spring, summer, and fall. About 60 % of the total land area in summer was cultivated land, whereas only 20 and 5 % of the total land area were cultivated land during fall and spring, respectively. The rest of the total land area was constantly covered with urban, forest, and water for the three seasons. The overall accuracy and kappa coefficient ranging from of 87 % to 92 % and 0.8 to 0.90 was obtained during accuracy assessment of the seasonal LULC data layers. This suggested that the seasonal data layers can reasonably be used in the Soil and Water Assessment Tool (SWAT) to analyze the effects of LULC data variation on hydrology and water quality of BSRW. SWAT was calibrated and validated for streamflow, sediment yield, and nutrient concentration using the summer LULC data layer and those parameters were applied to the models using the spring and fall LULC data layers. SWAT output for runoff, sediment yield, and nutrient load was found to be very sensitive to the change in LULC data layers. The average amount of runoff and sediment yield was higher during the summer while total nitrogen and total phosphorous yields were higher during the fall and spring, respectively. Agricultural operations are usually conducted during the summer and fields are mostly barren during the spring and fall. The use of seasonal LULC data layers is very beneficial to the scientific community as they can better explain the seasonal variation in hydrology and water quality as compared to the annual cropland data layer that is available for a single season of a year.

1. Introduction

The modification of the earth's surface caused by anthropogenic activities such as urbanization, deforestation, and agricultural practices or by natural phenomena such as floods, soil-erosion, landslides, and climate change are referred as land use and land cover (LULC) change (Abdulkareem et al., 2019; Hassan et al., 2016; Imran, 2019). Change in LULC is responsible for alterations in ecosystems and environmental processes at local, regional and global levels (Gebremicael et al., 2019; Gyamfi et al., 2016). Changes in LULC have led to global warming, loss of agricultural land, degradation of soil and water quality, expansion of urban areas, etc. (Hassan et al., 2016).Thus, LULC change is a very important topic of study as they relate to climate change, and changes in urbanization, agriculture, forestry, geology, hydrology, and other ecosystem services.

Assessment of the effects of LULC change on hydrology and water quality can provide critical inputs to the decision making during development of watershed management and ecological restoration strategies (Gyamfi et al., 2016; Hassan et al., 2016; Nie et al., 2011). To date, most of the research, on how LULC change affects hydrology and water quality, has been focused on evaluating changes in channel discharge in response to LULC change over a period of more than a decade (Dinka and Klik, 2019; Ghaffari et al., 2010; Hernandez et al., 2000). However, characteristics of agricultural land also vary seasonally, according to cropping and harvesting operations conducted in the watershed, each year. LULC change for an agricultural watershed like the Big Sunflower River watershed (BSRW) is a continuous process and the hydrological behavior of the watershed varies significantly for different seasons within a year. Thus, there is a need to study the changes in hydrology and water quality within the watershed as a response to the

* Corresponding author.
E-mail address: pparajuli@abe.msstate.edu (P.B. Parajuli).

https://doi.org/10.1016/j.agwat.2020.106366
Received 13 March 2020; Received in revised form 30 June 2020; Accepted 1 July 2020

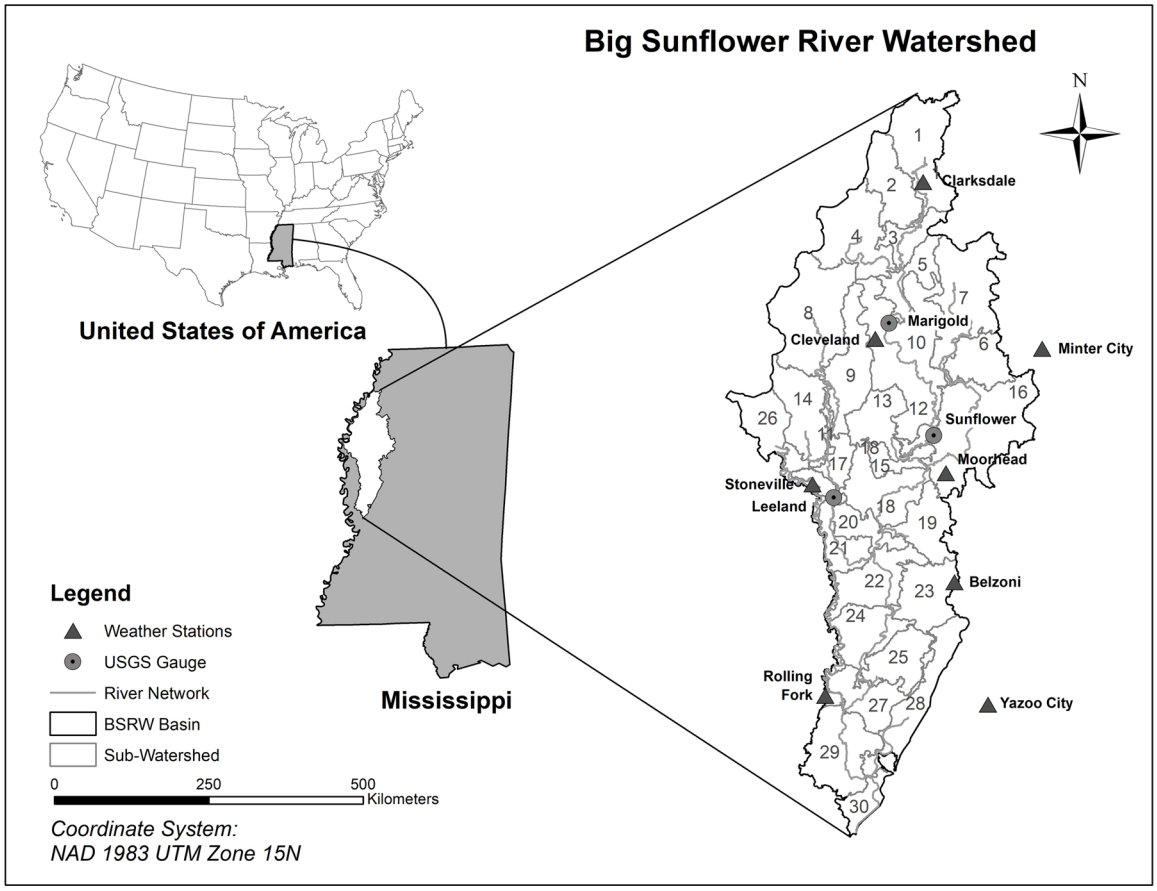

Fig. 1. Location map of Big Sunflower River Watershed in Mississippi, its sub-watersheds, river network, weather stations, and USGS gauges.

seasonal variations in the LULC data. Spring, summer and fall seasons were considered for the analysis of seasonal variation in the study area while winter was not been considered in this study as the climate of BSRW is characterized by very short duration of severe cold weather (NOAA NCEI, 2020).

LULC change analysis is usually performed using remote sensing data obtained using satellite imagery or aerial photographs. With the development of remote sensing technologies and the availability of satellite data such as Land remote-sensing satellite system (LANDSAT), Moderate resolution imaging spectral-radiometer (MODIS), and other spaceborne high resolution (HR) and very high resolution (VHR) sensors, effective methods have been developed for the analysis of land cover change (Goldblatt et al., 2018; Patel et al., 2015).

Much research has been conducted to quantify how climate and land use change impact the hydrologic cycle and water quality. For example, climate and land-use change impacts on streamflow, nitrogen, and phosphorus were examined for a Canadian river basin where a change in streamflow was due to climatic variability, whereas the change in nutrient concentration was due to alteration in land-use (El-Khoury et al., 2015). The hydrologic model, Soil and Water Assessment Tool (SWAT), incorporating spatial and temporal dynamics of land use and land cover, was effective in simulating streamflow, sediment and nutrient yield for Bagmati River Basin, located in Kathmandu, Nepal (Pokhrel, 2018). Impacts of LULC change in surface runoff, percolation, baseflow and evapotranspiration (ET) were evaluated for the upper San Pedro watershed located in Sonora, Mexico and southeastern Arizona, USA providing quantitative information to the stakeholders for better watershed management plan (Nie et al., 2011). A study conducted at Lake Tahoe, a sub-alpine lake, located in the state of California and Nevada, USA found that nutrients concentration varied according to the seasonal alterations in groundwater recharge (Naranjo et al., 2019).

Although there are numerous studies related to hydrology and water quality in response to long term LULC change, there is limited literature to date that evaluates watershed processes based on dominant seasonal LULC data (Dinka and Klik, 2019; Ghaffari et al., 2010; Hernandez et al., 2000).

The objectives of this study are to (a) develop a LULC data layers for spring, summer, and fall, (b) perform accuracy assessment of those data layers, and (c) use them in the SWAT model to analyze sensitivity of change in seasonal LULC data layers to streamflow, sediment yield, and nutrient load.

2. Material and methods

2.1. Study area

The area selected for this study is the BSRW, a major sub-watershed of the Yazoo River Basin, located within the lower part of Mississippi River Alluvial Plain, also known as Mississippi Delta. It lies in the northwestern part of Mississippi between the latitude of 32° 30′N to 34° 25′N and longitude of 91°10′E to 90°13′E. It covers an area of 10,500 km^2 and falls within ten different counties in Mississippi. Elevation of the BSRW watershed ranges from nearly flat to undulating gentle slopes from around 15–60 meters above mean sea level. It is an agricultural watershed, with agricultural fields covering about 70 % of the total land in BSRW. The major types of soil include Sharkey, Dowling, Forestdale, Alligator and Dundee, all of which have higher percentages of clay and silt. The location map of BSRW is shown in Fig. 1.

2.2. Landsat image

Landsat images from 2014 to 2018 were used to obtain seasonal

Table 1
Representation of error matrix for a data layer classification having five different classes.

Classified data layer	Reference data					Total
	Class 1	Class 2	Class 3	Class 4	Class 5	
Class 1	C_{11}	C_{12}	C_{13}	C_{14}	C_{15}	C_{1n}
Class 2	C_{21}	C_{22}	C_{23}	C_{24}	C_{25}	C_{2n}
Class 3	C_{31}	C_{32}	C_{33}	C_{34}	C_{35}	C_{3n}
Class 4	C_{41}	C_{42}	C_{43}	C_{44}	C_{45}	C_{4n}
Class 5	C_{51}	C_{52}	C_{53}	C_{54}	C_{55}	C_{5n}
Total	C_{n1}	C_{n2}	C_{n3}	C_{n4}	C_{n5}	C_{nn}

LULC data layers. Landsat satellites have been continuously providing images of the earth's land surface since 1972 (Goldblatt et al., 2018). The temporal resolution of the Landsat is 16 days. The Landsat Ecosystem Disturbance Adaptive Processing System (LEDAPS), a National Aeronautics and Space Administration (NASA) project, have processed the Landsat Thematic Mapper (TM) and Enhanced Thematic Mapper Plus (ETM +) imagery into surface reflectance scenes for North America using atmospheric correction procedures that was originally developed for the Moderate Resolution Imaging Spectroradiometer (MODIS) instruments (Masek et al., 2012, 2006). These surface reflectance scenes are very helpful for the research on LULC since it does not have atmospheric scattering or absorption and is measured at ground level. Cloud free Landsat 8 OLI Level-2 images, having higher image quality, were used in this study. They are generated using the Land Surface Reflectance Code (LaSRC) algorithm (Version 1.4.1), which makes use of the coastal aerosol band to perform aerosol inversion tests, auxiliary climate data from MODIS, and a radiative transfer model (Vermote et al., 2016). Landsat Level-2 surface reflectance image produced by USGS Landsat Science team are corrected for atmospheric errors such as aerosol scattering and thin clouds, and can be used directly for research purpose (USGS Landsat Missions, 2020). As the Landsat 8 data are available from 2013 till date, the images from 2014 to 2018 for each month were downloaded from USGS Global Visualization Viewer (https://glovis.usgs.gov) (GLOVIS, 2020). The Landsat 8 OLI has nine spectral bands including a panchromatic band. Band 1 to band 7 have a resolution of 30 m while band 8, a panchromatic band has a resolution on 15 m and band 9, a cirrus band has a resolution of 30 m. Bands 1–7 of the downloaded image were selected for this study. Those bands were layer stacked using ArcGIS after which the two scenes of the image for our watershed area were mosaicked and clipped using the watershed boundary.

2.3. LULC classification

Several parametric and non-parametric classification methods are available for LULC classification. Maximum likelihood (ML) method is one the extensively used parametric methods. It is based on Bayes' Theorem and assumes a single normal distribution of the samples per class in the feature space. Variances and covariances of the signatures classes are used to assign each raster-cell a pre-defined class (Ritchie et al., 2018). Different classes are characterized by the mean vector and the covariance matrix with the assumption that the distribution of a class sample is normal. Non-parametric classification methods like support vector machine (SVM) and random forest (RF) do not make any assumptions regarding data distribution and they do not require any statistical parameters to identify classes. SVM is based on concept of maximization and can be used for data with heterogeneous classes and limited numbers of training samples (Melgani and Bruzzone, 2004). Decision tree (DT) classification methods on the other hand divide a dataset into smaller subsets through tests defined at each part in the tree (Friedl and Brodley, 1997). DTs are further broken down into roots, nodes, and leafs. DTs are open-source software and thus can be helpful in lowering the cost of classification. Random forest classifier (RF) develops multiple decision trees in classifying images (Welch, 2019) and each decision tree is generated from different subsets of the training data. This method is comparatively accurate and can handle several input variables at a time (Peng et al., 2019).

The Maximum Likelihood(ML) Classification algorithm available in ArcGIS was applied to classify Landsat images to develop LULC data layers for each month in this study because of its robust abilities and its availability in almost every image processing software (Lu and Weng, 2007). These data layers were then combined to produce seasonal LULC data layers. This method is one of the widely used supervised classification techniques.

Multiple LULC data layers of BSRW for each month from 2014 to 2018 were developed by classifying cloud free Landsat images. The images were classified to water, forested wetlands, cultivated, barren, and urban. The year was divided into three seasons: January to April as spring, May to August as summer, and September to December as fall.

2.4. Development of seasonal LULC data layer

The numerical values were given to each class in the monthly LULC data layers. The data layers from 2014 to 2018 were then added together according to the months in spring, summer, and fall using raster calculator tool in ArcGIS. The resulting data layers were then reclassified again as water, forest, cultivated, barren, and urban according to resultant pixel value to produce dominant LULC data layers representing each season. Those seasonal LULC data layers were used in SWAT to analyze differences in runoff, sediment yield, and nutrient concentration due to changes in seasonal LULC data layers.

2.5. Accuracy assessment

The accuracy of the classification describes the agreement of classified image with reference to ground truth data and is performed generally using confusion or error matrix (Foody, 2002). The error matrix provides a cross-tabulation of a mapped classes against the ground truth reference data and helps to characterize accuracy metrices. The accuracy of the LULC data layers for each season was assessed by comparing the classified seasonal data layer with Landsat images of the respective seasons. A set of random points for ground truth data or reference data were created for the accuracy assessment using error matrix. Some of these points were also validated by visiting the study area. About 50 points for each class including water, forest, cultivated land, barren land, and urban areas were considered for accuracy assessment.

2.5.1. Error matrix and the accuracy Metrices

An error matrix is one of the quantitative methods for characterizing the accuracy of classified images. It is a square array denoting the correspondence between a classified data layer and the ground truth data. The rows in the matrix indicate the class of classified data layer while the columns indicate the ground truth data or reference data. A sample error matrix for five classes is shown in Table 1.

The diagonal values indicate the accuracy of the classification while non-diagonal values indicate the error between the classified data and its corresponding reference data. Producer's accuracy (PA), user's accuracy (UA), overall accuracy (OA), and kappa coefficient were computed using an error matrix. PA or the omission error (OE) gives the indication of accuracy of each class where pixels of a known class are classified as something other than that class. Similarly, UA or the commission error (CE) indicates the accuracy of each class where pixels are incorrectly classified as a known class when they should have been classified as something else.

2.5.1.1. Overall accuracy. The overall accuracy (OA) indicates the accuracy of all the classes included in image classification and

informs what proportion of the entire area is classified correctly. The diagonal cells of the error matrix contain the number of correctly classified pixels. The overall accuracy (OA) of the classification is obtained by dividing the sum of correctly classified pixels by the total number of reference pixels. It is usually expressed as a percent. From a similar error matrix generated in this study as shown in Table 1, the OA was calculated by summing the pixels in the diagonal and dividing them by total number of pixels in the error matrix as

$$OA = \frac{C_{11} + C_{22} + C_{33} + C_{44} + C_{55}}{N}$$

where C_{11}, C_{22}, C_{33}, C_{44}, and C_{55} are the correctly assigned pixels for each class; and N is the total number of pixels for all the classes considered in the accuracy assessment.

2.5.1.2. Kappa coefficient. The kappa coefficient is a measure of the difference between actual agreement and the agreement expected by chance. It is one of the standard measures used in accuracy assessment and has been recommended by several studies as it resolves the issue of correct allocation of a class by coincident (Foody, 2002; Rosenfield and Fitzpatrick-Lins, 1986; Smits et al., 1999). The kappa coefficient is generated using a statistical test and its value can vary from -1 to 1. A value less than 0 indicates that the classification is no better than a classification obtained by chance and a value near 1 indicates that the classification is significantly better than a classification obtained by chance. A kappa coefficient ≥ 0.80, represents strong agreement and good accuracy while a kappa coefficient ≤ 0.40 is considered poor (Rwanga and Ndambuki, 2017).

From a similar error matrix generated in this study as shown in Table 1, the kappa coefficient was computed by

$$kappa\ coefficient = \frac{N\sum_{i=1}^{k} C_{ii} - \sum_{i=1}^{k} (C_{i+} \times C_{+i})}{N^2 - \sum_{i=1}^{k} (C_{i+} \times C_{+i})}$$

where, C_{ii} is the correctly assigned pixel for ith class, C_{i+} marginal total of row for class i; C_{+i} is the marginal total of column for class i; k is the total number of classes; and N is the total number of pixels considered in accuracy assessment.

2.6. SWAT

SWAT is an extensively applied watershed scale model that can simulate hydrology and water quality and predict the impacts of different land use change and best management practices (BMPS) at a watershed scale (Neitsch et al., 2002). The modelling tool delineates the watershed using digital elevation model (DEM) and divides it into sub-basins. Sub-basins are further divided into hydrologic response units (HRUs), a unique combination of land use, soil, and slope, after incorporation of land use and soil data in the model. The time series data of precipitation, temperature, relative humidity, solar radiation, and wind speed along with management operation are provided to the model which helps in determination of quantities such as surface runoff, evapotranspiration, infiltration, sediment yield, groundwater recharge, water quality outputs etc. at each HRU, sub-basins and reach segments of the watershed (Neitsch et al., 2005, 2002).

The SWAT model has been successfully implemented in simulating streamflow, sediment yield, and the nutrient load from a watershed (Dakhlalla et al., 2016; Ni and Parajuli, 2018; Parajuli et al., 2013; Risal and Parajuli, 2019). Streamflow is the discharge of water in streams or any water body and is one of the main components of runoff generated from the land surface. In SWAT, streamflow is estimated using SCS curve number method (Neitsch et al., 2005). The sediment eroded by sheet, rill, gully, and streambank erosion are transported through the streams and are estimated in SWAT using the Modified Universal Soil Loss Equation (MUSLE) (Neitsch et al., 2005). Similarly, nutrients like nitrogen and phosphorous are the essential micro-nutrients required for crop growth the excess amount of these nutrients, transported to the water body, severely deteriorates the water quality of streams, rivers, lakes and shallow groundwater (Lory, 2018). They are estimated in SWAT considering their supply and demand (Neitsch et al., 2005).

In the current study, three seasonal LULC data layers were individually applied to the SWAT with other inputs being same in order to analyze difference in streamflow, sediment yield, and nutrient concentration as response to the seasonal LULC change.

2.6.1. SWAT input

SWAT input requirements include: Digital Elevation Model (DEM), LULC data layer, Soil fata layer, and daily time-series of meteorological data such as precipitation, maximum and minimum temperature, relative humidity, solar radiation, and wind speed. A 30 m resolution DEM of 3D Elevation Program (3DEP) series, provided by United States Geological Survey (USGS, 2020), was obtained from National map viewer (http://viewer.nationalmap.gov).

Soil Survey Geographic (SSURGO) data was obtained from United States Department of Agriculture (USDA), Natural Resource Conservation Service (NRCS) (https://www.nrcs.usda.gov) (NRCS, 2020). Meteorological data was derived from National Oceanic and Atmospheric Administration (NOAA) (https://www.ncdc.noaa.gov) (NOAA NCEI, 2020).

2.6.2. SWAT calibration and validation

Multisite SWAT calibration and validation was performed for streamflow, sediment yield, total nitrogen and total phosphorous at the outlets of sub-basin 5, sub-basin 10 and sub-basin 17 of BSRW situated at the USGS gauges 728,820 (Marigold), 7,288,500 (Sunflower) and 788,650 (Leland) respectively as shown in Fig. 1. Streamflow was calibrated from January 2013 to December 2015 and validated from January 2016 to December 2019 using observed monthly discharge obtained from the three USGS gauges. Similarly, sediment yield, total nitrogen, and total phosphorous were calibrated from November 2013 to December 2014 and validated from January 2015 to December 2016 at the outlets of sub-basin 5, sub-basin 10, and sub-basin. Calibration and validation were based on measured daily total suspended solid (TSS), total nitrogen (TN), and total phosphorous (TP). These data were obtained every fifteen days from 2013 to 2016. The calibration and validation period for sediment yield, total nitrogen, and total phosphorous was shorter than that for streamflow because of the limitation of observed data.

Automatic calibration of streamflow, sediment yield, total nitrogen, and total phosphorous was performed using the Sequential Uncertainty Fitting (SUFI-2) algorithm within SWAT Calibration and Uncertainty Procedures (SWAT-CUP) package (Abbaspour, 2013). The R-factor and P-factor, which were computed by SUFI-2, were used to predict model uncertainty. T-statistics and P-value were used to perform sensitivity analysis.

The model performance during calibration and validation was analyzed using the coefficient of determination (R^2) (Draper and Smith, 1966), and Nash Sutcliffe Efficiency (NSE) (Nash and Sutcliffe, 1970). These two statistics are widely used and reliable measures for comparing observed and simulated data. The value of NSE ranges from $-\infty$ to 1 and R^2 ranges from 0 to 1. Values of 1, for both statistics, are considered perfect (Krause et al., 2005; Nash and Sutcliffe, 1970). In general, if NSE is greater than 0.50, model simulation can be considered as satisfactory (Moriasi et al., 2007).

The parameters used, their range, and the calibrated values for streamflow, sediment yield, total nitrogen, and total phosphorous are shown in Table 2.

Table 2
SWAT parameters for the calibration of streamflow, sediment yield, total nitrogen and total phosphorous in the Big sunflower river watershed.

Variable	Parameters[a]	Description	Fitted value	Minimum value	Maximum value
Streamflow	r_CN2.mgt	Initial SCS runoff curve number for moisture condition II	−0.09	−0.24	0.05
	v_ALPHA_BF.gw	Base flow alpha factor (days)	0.14	−0.28	0.57
	v_GW_DELAY.gw	Groundwater delay (days)	516.07	273.02	759.10
	v_GWQMN.gw	Threshold depth of water in the shallow aquifer for return flow to occur (mm H2O)	1.34	0.67	2.01
	r_SOL_AWC(1).sol	Available water capacity of first soil layer	0.37	0.05	0.68
	v_ESCO.bsn	Soil evaporation compensation factor	1.05	0.67	1.42
	v_CH_N2.rte	Manning's n (roughness) for channel	0.35	0.07	0.62
	v_GW_REVAP.gw	Groundwater re-evaporation coefficient	1.07	0.53	1.59
	v_SURLAG.bsn	Surface runoff lag time (days)	8.37	2.55	14.18
Sediment yield	v_CH_COV1.rte	Channel cover factor 1	0.27	0.12	0.53
	v_CH_COV2.rte	Channel cover factor 2	0.61	0.48	0.61
	v_CH_ERODMO().rte	Monthly channel erodibility factor	0.53	0.48	1.03
	v_SPEXP.bsn	Exponent parameter for calculating sediment re-entrained in channel	1.10	0.96	1.28
	v_SPCON.bsn	Linear parameter for calculating the maximum amount of sediment re-entrained during channel sediment routing	0.00	−0.01	0.00
	v_USLE_P.mgt	Universal Soil Loss Equation (USLE) management practice factor	0.87	0.84	1.29
	r_SLSUBBSN.hru	Average slope length	0.44	0.19	0.41
	r_HRU_SLP.hru	Average slope steepness	−0.99	−1.37	−0.77
	r_USLE_K(1).sol	Universal Soil Loss Equation (USLE) soil erodibility factor of first soil layer	0.46	0.02	0.55
Total nitrogen	v_RCN.bsn	Concentration of nitrogen in rainfall	2.51	1.05	3.96
	v_NPERCO.bsn	Nitrogen percolation coefficient	0.01	−0.24	0.26
	v_BC3.swq	Rate constant for hydrolysis of organic nitrogen to NH4 in reach	0.41	0.32	0.49
	v_RS3.swq	Benthic source rate for NH4-N in reach	2.67	1.96	3.38
	v_RS4.swq	Rate coefficient for organic nitrogen settling in reach	0.39	0.27	0.51
	v_ERORGN.hru	Organic nitrogen enrichment ratio	3.03	2.25	3.82
Total Phosphorous	v_CMN.bsn	Humus mineralization rate factor of active organic nutrient	0.001	0.001	0.003
	v_PHOSKD.bsn	Phosphorus soil partitioning coefficient	119.40	100	300
	v_PPERCO.bsn	Phosphorus percolation coefficient	12.81	10	15
	v_BC4.swq	Rate constant for decay of organic phosphorus to dissolved phosphorus	0.17	0.01	0.7
	v_RS2.swq	Benthic source rate for dissolved phosphorus in reach	0.39	0.005	0.5
	v_RS5.swq	Organic phosphorus settling rate in reach	0.05	0.05	1

[a] V_ indicates existing parameter was replaced by the fitted value, and r_ indicates existing parameter value is multiplied by (1 + fittedvalue).

3. Results

3.1. Seasonal LULC data layer

The LULC data layer from summer showed that about 60 % of the total land was cultivated whereas the percentage of cultivated land during fall and spring were just 20 % and 5%, respectively. The majority of the agricultural lands during spring and fall were barren. The percentage of urban, forest, and water, for all three seasons, was almost constant with around 21 %, 12 % and 1 %, respectively. The seasonal LULC data layers for spring, fall, and summer are shown in Fig. 2.

3.2. Accuracy of seasonal data layer

The seasonal LULC data layer for all three seasons were characterized by higher precision with overall accuracy ranging from of 87% to 92% and kappa coefficient ranging from 0.84 to 0.90. The producer's accuracy and user's accuracy for different classes ranged from 68 % to 100 % and 75% to 100 %, respectively. The different accuracy matrices for summer, fall and spring are summarized in Table 3.

3.3. Model performance

3.3.1. Streamflow

For the calibration of streamflow, nine parameters were used. Among them, four parameters namely: initial SCS runoff curve number for moisture condition II (CN2), available water capacity of first soil layer (SOL_AWC (1)), ground water delay (GW_DELAY), and manning's roughness coefficient for channel (CH_N2) were highly sensitive having an absolute value of a T-stat greater than 4 and a P-value less than 0.0001. The groundwater re-evaporation coefficient (GW_REVAP) was the least sensitive parameter with a T-stat of 0.33 and a P-value of 0.7.

The statistics obtained during the calibration and validation of streamflow were reasonable with an R^2 ranging from 0.65 to 0.92 and an NSE ranging from 0.60 to 0.91. The summary of statistics for calibration and validation of streamflow at sub-basin 5, sub-basin 10, and sub-basin 17 of BSRW are presented in Table 4 and the graph showing time series of observed and simulated streamflow during its calibration and validation at sub-basin 5 is presented in Fig. 3.

3.3.2. Sediment yield

For the calibration of sediment yield, nine parameters were used. Among them, five parameters namely: average slope steepness (HRU_SLP), universal soil loss equation- soil erodibility factor of first soil layer (USLE_K (1)), universal soil loss equation-management practice factor (USLE_P), channel cover factor 2(CH_COV2), and monthly channel erodibility factor (CH_ERODMO) were highly sensitive with absolute value of a T-stat greater than 2 and a P-value less than 0.02. The exponent parameter for calculating sediment re-entrained in channel (SPEXP) was the least sensitive with a T-stat of 0.09 and a P-value of 0.9.

The statistics obtained during the calibration a nd validation of sediment yield were satisfactory with an R^2 ranging from 0.59 to 0.75 and an NSE ranging from 0.30 to 0.48. The statistics obtained during calibration and validation of sediment yield at sub-basin 5, sub-basin 10, and sub-basin 17 of BSRW are summarized in Table 5 and the graph showing time series of observed and simulated sediment yield during its calibration and validation at sub-basin 5 is presented in Fig. 4.

3.3.3. Total nitrogen

For the calibration of total nitrogen, six parameters were used. Among them, the nitrogen percolation coefficient (NPERCO) and the concentration of nitrogen in rainfall (RCN) were highly sensitive with a T-stat greater than 2 and a P-value less than 0.01. The benthic source rate for NH4-N in reach (RS3) was the least sensitive parameter with a T-stat of -0.5 and a P-value of 0.5.

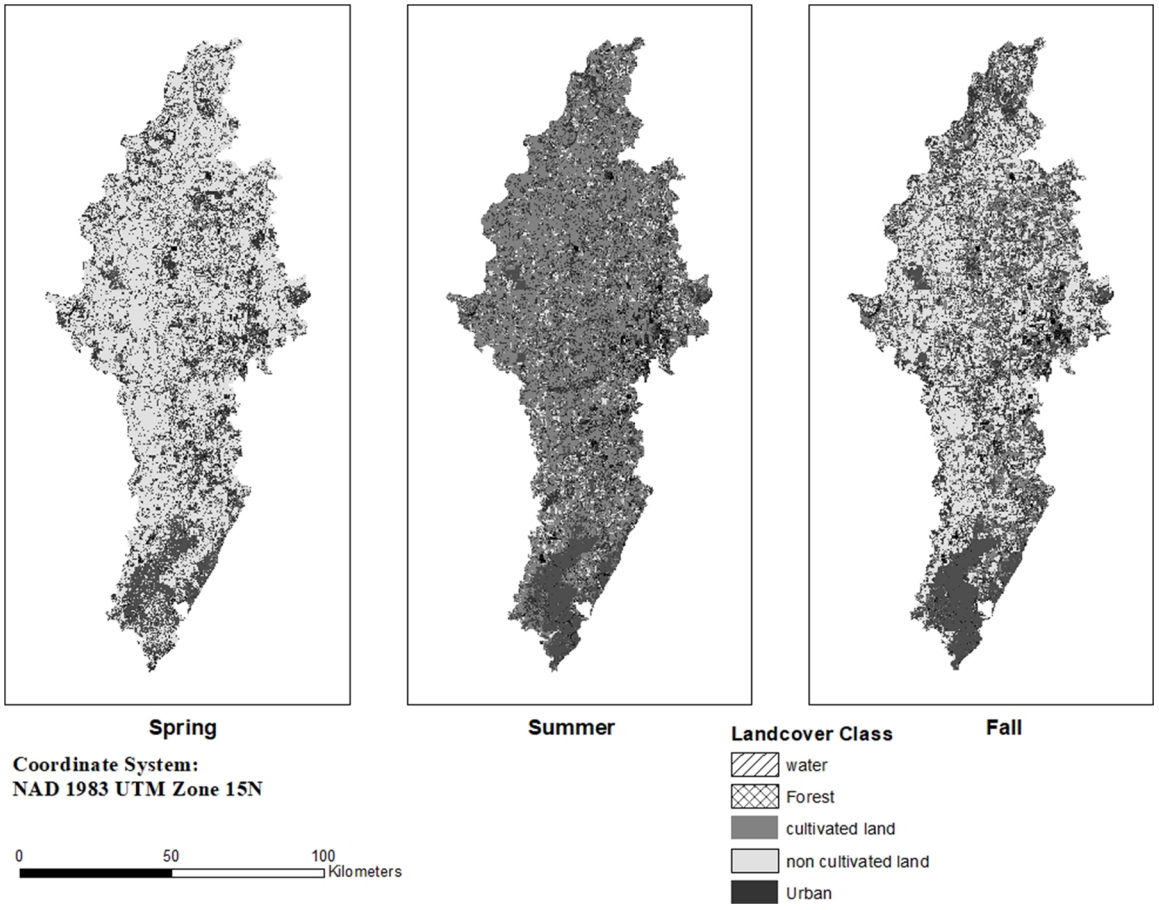

Fig. 2. The land-use and land-cover data layer for spring (January to April), summer (May to August), and fall (September to December).

The R^2 and NSE obtained during the calibration and validation of total nitrogen were satisfactory with an R^2 ranging from 0.45 to 0.80 and a NSE ranging from 0.19 to 0.69. The summary of statistics obtained during calibration and validation of total nitrogen at sub-basin 5, sub-basin 10, and sub-basin 17 of BSRW are presented in Table 6 and the graph showing time series of observed and simulated total nitrogen load during its calibration and validation at sub-basin 5 is presented in Fig. 5.

Table 4
Statistics obtained during calibration and validation of streamflow at the outlet of three sub-basins of Big Sunflower River watershed.

	Calibration		Validation	
	R^2	NSE	R^2	NSE
Sub-basin 5	0.76	0.62	0.65	0.60
Sub-basin 10	0.79	0.75	0.75	0.74
Sub-basin 17	0.77	0.75	0.92	0.91

3.3.4. *Total phosphorous*

For the calibration of total phosphorous, six parameters were used. Among them, the rate constant for decay of organic phosphorus to dissolved phosphorus (BC4), phosphorus soil partitioning coefficient (PHOSKD), and phosphorus percolation coefficient (PPERCO) were seen to be highly sensitive with the T-stat greater than 2.6 and a P-value less than 0.009 while the humus mineralization rate factor of active organic nutrient (CMN) was found to be the least sensitive with the T-stat of 0.6 and a P-value of 0.5.

The calibration and validation statistics of total phosphorous were satisfactory with an R^2 ranging from 0.67 to 0.91 and an NSE ranging from 0.49 to 0.77. A summary of calibration and validation statistics of total phosphorous at sub-basin 5, sub-basin 10, and sub-basin 17 of BSRW are presented in Table 7 and the graph showing time series of observed and simulated total phosphorous load during its calibration

Table 3
Accuracy metrices of individual class, Overall accuracy and Kappa coefficient for summer fall and spring.

Class	Summer		Fall		Spring	
	Producer's Accuracy	User's Accuracy	Producer's Accuracy	User's Accuracy	Producer's Accuracy	User's Accuracy
Water	0.81	1.00	0.81	1.00	0.94	1.00
Forest	1.00	1.00	0.94	0.98	0.80	0.98
Cultivated land	0.98	0.76	0.90	0.87	0.94	0.88
Barren land	0.68	0.96	0.98	0.90	1.00	0.80
Urban	0.91	0.75	0.95	0.89	0.87	0.95
Overall Accuracy		0.87		0.92		0.91
Kappa Coefficient		0.84		0.90		0.88

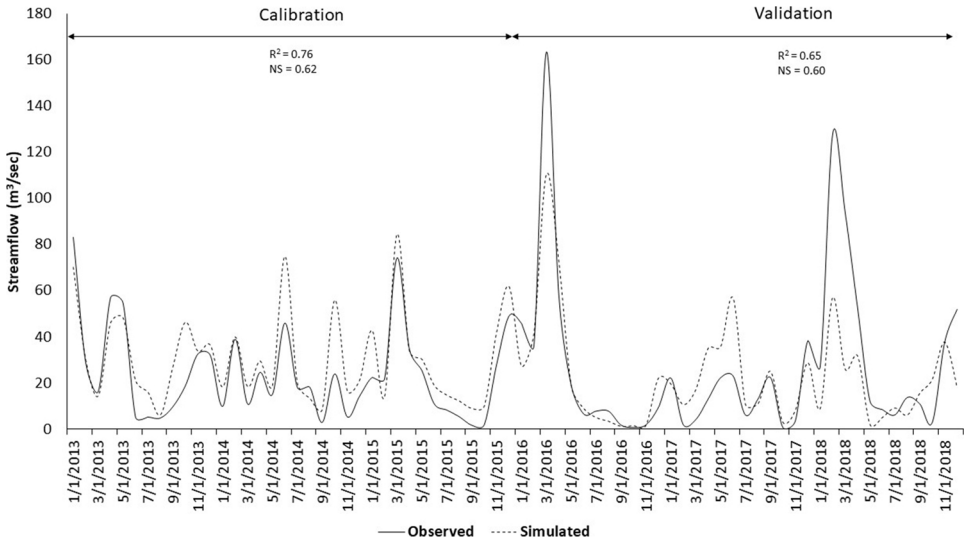

Fig. 3. Observed and simulated streamflow during calibration and validation of streamflow at sub-basin 5 of Big Sunflower River watershed.

Table 5
Statistics obtained during calibration and validation of sediment yield at the outlet of three sub-basins of Big Sunflower River watershed.

	Calibration		Validation	
	R^2	NSE	R^2	NSE
Sub-basin 5	0.75	0.48	0.59	0.30
Sub-basin 10	0.67	0.42	0.72	0.31
Sub-basin 17	0.59	0.39	0.66	0.32

Table 6
Statistics obtained during calibration and validation of total nitrogen at the outlet of three sub-basins of Big Sunflower River watershed.

	Calibration		Validation	
	R^2	NSE	R^2	NSE
Sub-basin 5	0.59	0.32	0.45	0.20
Sub-basin 10	0.78	0.31	0.33	0.19
Sub-basin 17	0.80	0.69	0.48	0.23

and validation at sub-basin 5 is presented in Fig. 6.

3.4. Effect of seasonal LULC data layers

3.4.1. Streamflow

The average streamflow was slightly higher during summer for all the four sub-watersheds than that during spring and fall. The average streamflow at the watershed outlet was observed to be 185.75 m^3/sec in summer while that for spring and fall were 164.82 m^3/sec and 181.12 m^3/sec respectively. Average streamflow at the outlet of sub-watersheds 5,10,17, and 30 of BSRW for spring, summer and fall seasons are shown in Fig. 7.

The average precipitation in the BSRW was highest in spring (636 mm) while rainfall during summer and fall were 439 mm and 455 mm respectively. The average monthly precipitation was highest during March and April (182 mm and 176 mm respectively) and lowest during September and August (84 mm and 93 mm respectively).

3.4.2. Sediment yield

The average sediment concentration was higher in summer for all the sub-watersheds in comparison to that in spring and fall despite the reduced average rainfall during summer. The average sediment concentration at the watershed outlet was observed to be 10.92 mg/L in summer while that for spring and fall were 3.10 mg/L and 3.27 mg/L

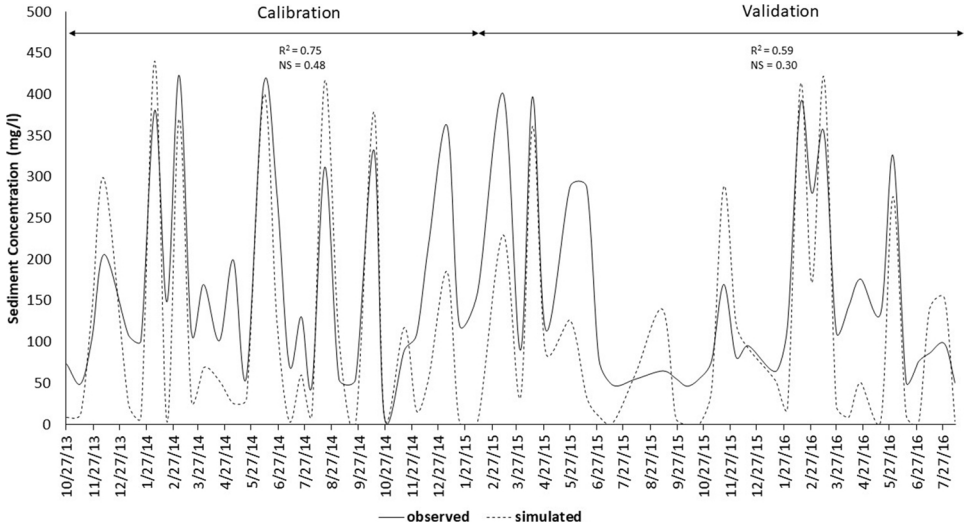

Fig. 4. Observed and simulated sediment yield during calibration and validation of sediment yield at sub-basin 5 of Big Sunflower River watershed.

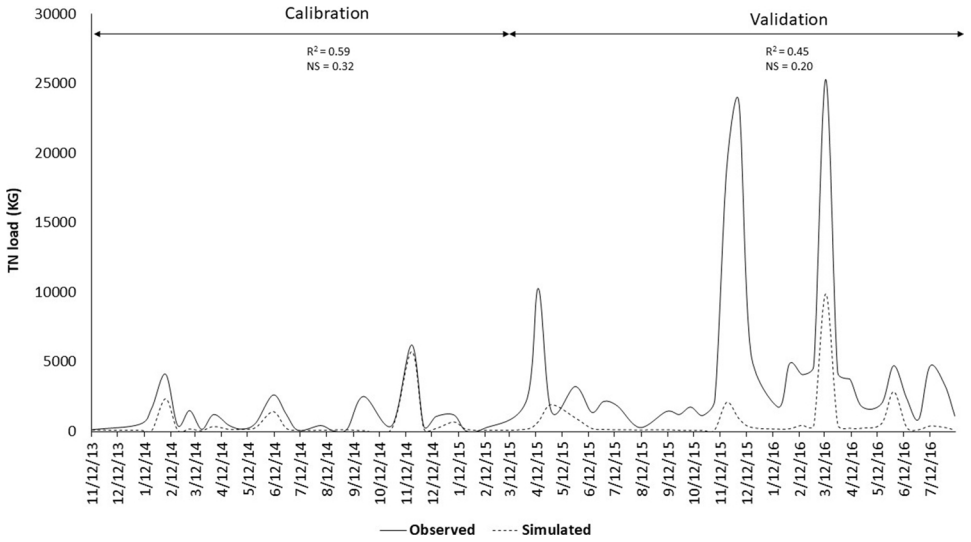

Fig. 5. Observed and simulated total nitrogen load during calibration and validation of total nitrogen at sub-basin 5 of Big Sunflower River watershed.

Table 7
Statistics obtained during calibration and validation of total phosphorous at the outlet of three sub-basins of Big Sunflower River watershed.

	Calibration		Validation	
	R^2	NSE	R^2	NSE
Sub-basin 5	0.85	0.77	0.67	0.65
Sub-basin 10	0.91	0.51	0.80	0.75
Sub-basin 17	0.81	0.49	0.67	0.56

respectively. Average sediment concentration at the outlet of sub-basin 5, 10, 17, and 30 for spring, summer and fall are shown in Fig. 8.

Although average precipitation was lower during the summer than spring or fall, average sediment concentration was higher during the summer. This is due to tillage during late spring and early summer before planting. In addition, increased flow from irrigation is responsible for higher soil erosion and sediment yield in the BSRW. Although conservation tillage practices such as no-till, strip-till, and mulch-till are encouraged to reduce soil erosion, more than 75 % farmers in Mississippi Delta still use conventional tillage prior to planting corn and soybean to create uniform seedbed and eliminate competition from weeds (Snipes et al., 2005).

Tillage induces soil erosion and is one of the responsible factors for the increase in sediment yield from agricultural watersheds (Zhao et al., 2018). This watershed scale study was conducted to assess the impact of tillage practices on stream flow, crop and sediment yields at the BSRW, Mississippi. Results show that conventional tillage produced higher sediment yield than reduced tillage (Parajuli et al., 2016).

3.4.3. Total nitrogen

The average total nitrogen concentration during fall was higher compared to the spring and summer for all four sub-watersheds. The average total nitrogen concentration at the watershed outlet was 136 Mg in the fall while that for spring and summer were 54 Mg and 92 Mg respectively. Average total nitrogen concentration at the outlets of sub-basins 5, 10, 17, and 30 for spring, summer and fall are shown in Fig. 9.

3.4.4. Total phosphorous

The average amount of total phosphorous concentration was higher in spring compared to summer and fall. The average total phosphorous yield at the watershed outlet was 325 Mg in spring while that for summer and fall were 245 Mg and 285 Mg respectively. Average total phosphorous concentrations at the outlet of sub-basins 5, 10, 17 and 30 for spring, summer and fall are shown in Fig. 10.

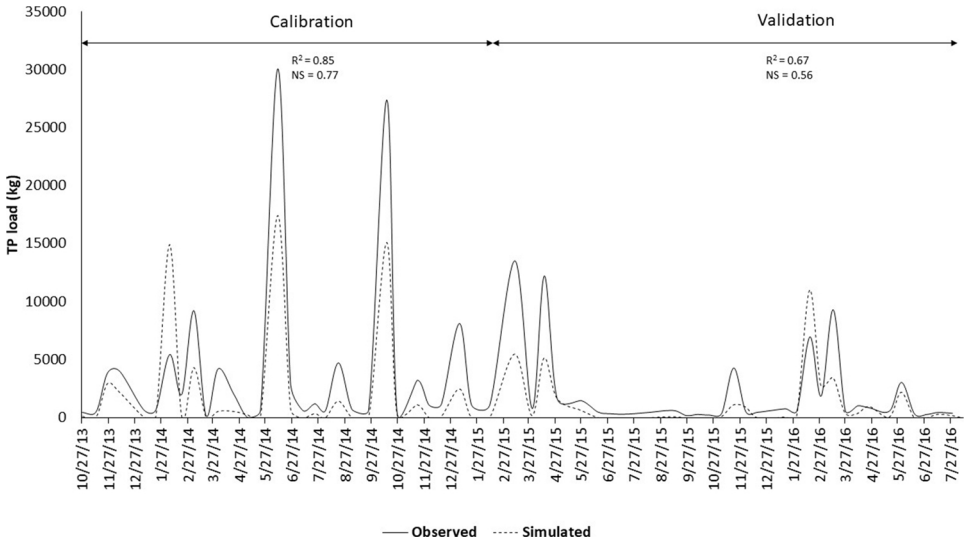

Fig. 6. Observed and simulated total phosphorous load during calibration and validation of total phosphorous at sub-basin 5 of Big Sunflower River watershed.

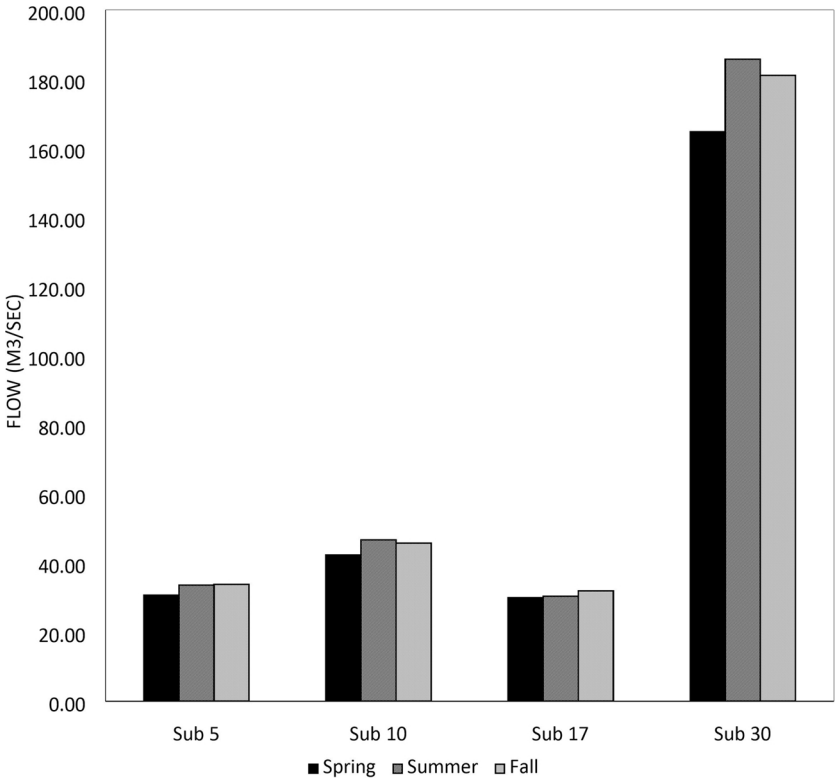

Fig. 7. Average streamflow at four sub-basins of the Big Sunflower River watershed for spring, summer and fall.

4. Discussion and conclusions

This study investigated the variation in surface runoff, sediment, and nutrient yield due to seasonal changes in land use and land cover for an agricultural watershed. This was accomplished by using multiple LULC data layers for three different seasons in the SWAT model. These kinds of seasonal variations cannot be observed using a single LULC data layer such as the cropland data layer (CDL) or the national land cover dataset (NLCD), as they use the LULC data layer created mostly from the images taken in summer.

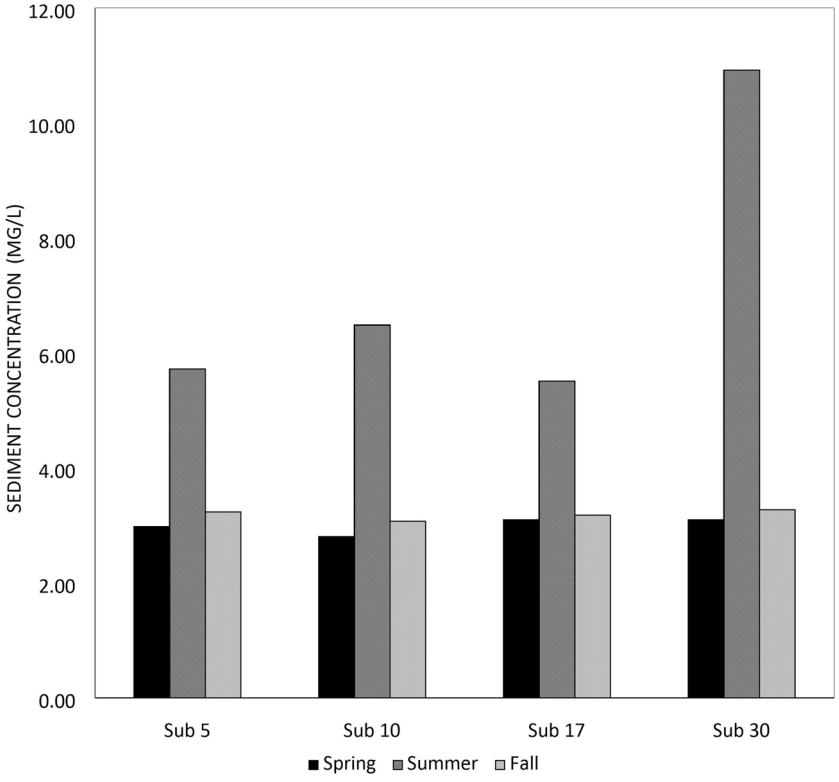

Fig. 8. Average sediment concentration at three calibrating sub-basins of Big Sunflower river watershed for spring, summer and fall.

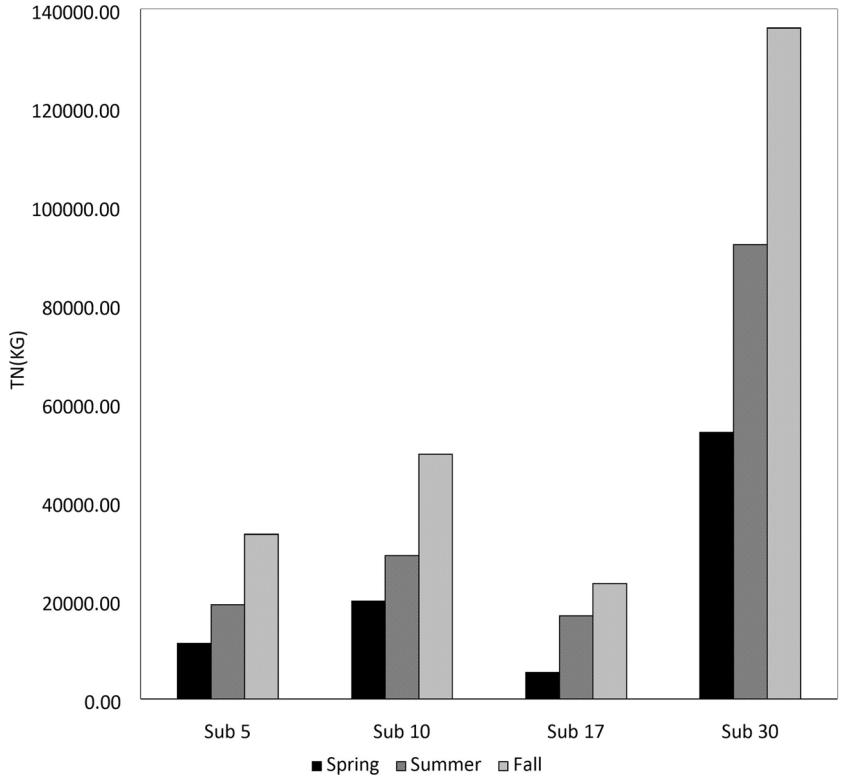

Fig. 9. Average total nitrogen concentration at three sub-basins of the Big Sunflower River watershed for spring, summer and fall.

The seasonal LULC data layers for spring, summer, and fall were obtained by combining monthly LULC data layers whose overall accuracy ranged between 87 % and 92 % and the kappa coefficient ranged between 0.84 to 0.90. These statistics suggest that the classified data layers generated represented respective seasons well. Three seasonal LULC data layers were used in SWAT and three separate models were developed.

The SWAT model was calibrated and validated for streamflow, sediment yield, total nitrogen and total phosphorous. The statistical values of R^2 and NSE obtained during the calibration and validation of

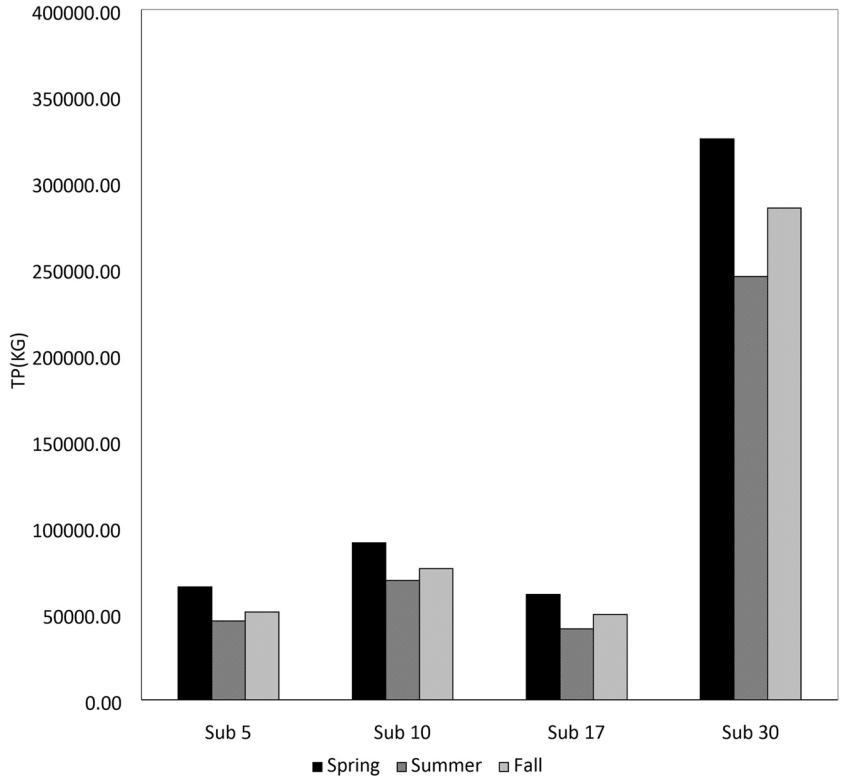

Fig. 10. Average total phosphorous concentration at three sub-basins of the Big Sunflower River watershed for spring, summer and fall.

streamflow was in accordance to the results of previous modelling studies conducted in the BSRW (Dakhlalla et al., 2016; Ni and Parajuli, 2018; Parajuli et al., 2016; Risal and Parajuli, 2019). Calibration and validation statistics were not much affected by the change in seasonal LULC data layer and were reasonable according to the standard set in a comprehensive review article based on more than 250 worldwide SWAT application studies (Gassman et al., 2007). Similarly, the statistics during simulation of sediment yield were also reasonable as sediment loading is driven by surface runoff and streamflow (Qi et al., 2020). The calibration and validation of sediment concentration at the three USGS gauging stations within BSRW were also found to be consistent with the previous SWAT calibration and validation results (Dakhlalla et al., 2016; Ni and Parajuli, 2018; Risal and Parajuli, 2019). Likewise, the calibration and validation of TN and TP were found satisfactory except for few exceptions caused by limitation of observed data (Moriasi et al., 2007). The observed data at certain periods were abnormally high and were responsible for lower value of statistics. The TN and TP simulations were consistent with previous calibration and validation results for BSRW (Risal and Parajuli, 2019). Even though it is desirable to calibrate the major constituents of nitrogen and phosphorous loading such as organic nitrogen/phosphorous and mineral nitrogen/phosphorous rather than TN and TP, the individual constituents could not be calibrated due to the unavailability of monitoring data for each constituent (Arnold et al., 2012).

The average streamflow at the watershed outlet during summer (185 m^3/sec) was highest than the average streamflow during spring (164 m^3/sec) and fall (181 m^3/sec) even though the average rainfall received during summer (439 mm) was lower than the average rainfall received during spring (636 mm) and fall (455 mm). This is due to the additional irrigation supplied to the fields through groundwater pumping. Due to the seasonal distribution of rainfall in BSRW region, supplemental irrigation is required to maximize crop yield. The crops in BSRW were planted in late April, harvested in early September and irrigated periodically during July to early August. The application of irrigation in the field was simulated using the auto-irrigation function of SWAT. Similarly, a study conducted in 18 Indian sub-continental river basins showed that irrigation is responsible for increases in surface runoff and streamflow in an agricultural watershed (Shah et al., 2019). The observed flow data also suggests greater flows in summer compared to fall or spring. Apart from increased crop productivity through required water supply during the dry period of the year, irrigation may also lead to increase in surface runoff and sediment transport if the method of irrigation is not appropriate (Peddi and Kumar, 2019; Raeisi-Vanani et al., 2017).

Like streamflow, average sediment concentration at the watershed outlet was highest during summer (10.92 mg/L) than during spring (3.10 mg/L) and fall (3.27 mg/L). This is due to the tillage operation conducted during late spring and early summer before planting. In addition, increased flow from irrigation is responsible for higher soil erosion and sediment yield in the BSRW. Although conservation tillage practices such as no-till, strip-till, and mulch-till are encouraged to reduce soil erosion, more that 75 % of farmers in the Mississippi Delta still use conventional tillage prior to planting corn and soybean to create uniform a seedbed and eliminate competition from weeds (Snipes et al., 2005). Tillage induces soil erosion and is one of the responsible factors for the increase in sediment yield from an agricultural watershed (Zhao et al., 2018). A previous watershed scale study conducted to assess the impact of tillage practices on stream flow, crop and sediment yields at the BSRW, Mississippi showed that conventional tillage produced higher sediment yield than reduced tillage (Parajuli et al., 2016).

On the other hand, average total nitrogen yield was lowest during spring (54 Mg) and highest during fall (136 Mg) due to the inability of plants to uptake all of the nitrogen fertilizer and washing off of unused nitrogen after runoff events. Nitrogen is added to the soil by different means such as fertilizer application, manure and plant residue application, rainfall, or fixation by symbiotic and non-symbiotic bacteria. Nitrogen is removed from the soil through plant uptake, leaching, denitrification, volatilization, and erosion. (Neitsch et al., 2005). Mineral nitrogen applied to corn and cotton during the last week of April and the crop residues left in the field after harvest in early September are responsible for high level of total nitrogen during the fall as only a small portion of applied fertilizer is up-taken by crops (Moreno et al., 2018). Moreover, crop residue left on the field in the fall after harvest also contributes total nitrogen washoff during runoff caused by rainfall.

Likewise, the average total phosphorous at the watershed outlet was highest in spring (325 Mg) and lowest in summer (245 Mg) due to the soluble nature of phosphorous which becomes readily available for transport in surface runoff and the ability of crops like soybean to accumulate phosphorous in the soil. Phosphorous is applied to soil through fertilizer, manure, and residue and removed by soil through plant uptake and erosion. The average amount of precipitation during the spring was higher than that in summer and fall. The total phosphorous concentration was also highest in spring. Phosphorous is highly soluble in water and is readily available for transport with surface runoff (Neitsch et al., 2005). Unlike nitrogen which is usually considered mobile, phosphorous is capable of easily combining with other ions to form insoluble compounds and precipitate out of soil and wash off with rainwater. The phosphorous present in the soil was mostly discharged by surface runoff during heavy rainfall events in the spring (Neitsch et al., 2005; Sharpley and Syers, 1979). As the major crop grown in the BSRW is soybeans, which is capable of accumulating soil phosphorous (Reddy et al., 1999), the total phosphorous concentration was lowest throughout summer during which the fields were planted with soybean.

This study is very valuable to the scientific community as it explains the variability of hydrologic and water quality components within a year not only due to changes in hydrology and agricultural practices, but also due to seasonal changes in land-use and land-cover patterns.

Declaration of Competing Interest

The authors declare that they have no known competing interest.

Acknowledgement

We would like to acknowledge the financial support of AFRI competitive grant award # 2017-67020-26375 from the USDA/NIFA for this project. We would like to acknowledge the support of USGS; Yazoo Mississippi Delta Joint Water Management District; and all our collaborators for providing necessary data and technical support during the study.

Appendix A. Supplementary data

Supplementary material related to this article can be found, in the online version, at doi:https://doi.org/10.1016/j.agwat.2020.106366.

References

Abbaspour, K.C., 2013. SWAT-CUP 2012. SWAT Calibration Uncertain. Progr.
Abdulkareem, J.H., Pradhan, B., Sulaiman, W.N.A., Jamil, N.R., 2019. Prediction of spatial soil loss impacted by long-term land-use/land-cover change in a tropical watershed. Geosci. Front. 10, 389–403. https://doi.org/10.1016/j.gsf.2017.10.010.
Arnold, J.G., Moriasi, D.N., Gassman, P.W., Abbaspour, K.C., White, M.J., Srinivasan, R., Santhi, C., Harmel, R.D., Van Griensven, A., Van Liew, M.W., 2012. SWAT: model use, calibration, and validation. Trans. ASABE 55, 1491–1508.
Dakhlalla, A.O., Parajuli, P.B., Ouyang, Y., Schmitz, D.W., 2016. Evaluating the impacts of crop rotations on groundwater storage and recharge in an agricultural watershed. Agric. Water Manag. 163, 332–343. https://doi.org/10.1016/j.agwat.2015.10.001.
Dinka, M.O., Klik, A., 2019. Effect of land use–land cover change on the regimes of surface runoff—the case of Lake Basaka catchment (Ethiopia). Environ. Monit. Assess. 191, 278.
Draper, N.R., Smith, H., 1966. Applied regression analysis, New York, 1966. EM Pugh GH Winslow, Anal. Phys. Meas. Addison-Wesley, New York, pp. 26.
El-Khoury, A., Seidou, O., Lapen, D.R., Que, Z., Mohammadian, M., Sunohara, M.,

Bahram, D., 2015. Combined impacts of future climate and land use changes on discharge, nitrogen and phosphorus loads for a Canadian river basin. J. Environ. Manage. 151, 76–86.
Foody, G.M., 2002. Status of land cover classification accuracy assessment. Remote Sens. Environ. 80, 185–201.
Friedl, M.A., Brodley, C.E., 1997. Decision tree classification of land cover from remotely sensed data. Remote Sens. Environ. 61, 399–409.
Gassman, P.W., Reyes, M.R., Green, C.H., Arnold, J.G., 2007. The soil and water assessment tool: historical development, applications, and future research directions. Trans. ASABE 50, 1211–1250.
Gebremicael, T.G., Mohamed, Y.A., Van der Zaag, P., 2019. Attributing the hydrological impact of different land use types and their long-term dynamics through combining parsimonious hydrological modelling, alteration analysis and PLSR analysis. Sci. Total Environ. 660, 1155–1167. https://doi.org/10.1016/j.scitotenv.2019.01.085.
Ghaffari, G., Keesstra, S., Ghodousi, J., Ahmadi, H., 2010. SWAT-simulated hydrological impact of land-use change in the Zanjanrood basin, Northwest Iran. Hydrol. Process. An Int. J. 24, 892–903.
GLOVIS, 2020. USGS,GLOVIS. [WWW Document]. URL. http://earthexplorer.usgs.gov/.
Goldblatt, R., Stuhlmacher, M.F., Tellman, B., Clinton, N., Hanson, G., Georgescu, M., Wang, C., Serrano-Candela, F., Khandelwal, A.K., Cheng, W.-H., Balling, R.C., 2018. Using Landsat and nighttime lights for supervised pixel-based image classification of urban land cover. Remote Sens. Environ. 205, 253–275. https://doi.org/10.1016/j.rse.2017.11.026.
Gyamfi, C., Ndambuki, J.M., Salim, R.W., 2016. Hydrological responses to land use/cover changes in the Olifants Basin, South Africa. Water 8, 588.
Hassan, Z., Shabbir, R., Ahmad, S.S., Malik, A.H., Aziz, N., Butt, A., Erum, S., 2016. Dynamics of land use and land cover change (LULCC) using geospatial techniques: a case study of Islamabad Pakistan. Springerplus 5, 812.
Hernandez, M., Miller, S.N., Goodrich, D.C., Goff, B.F., Kepner, W.G., Edmonds, C.M., Jones, K.B., 2000. Modeling runoff response to land cover and rainfall spatial variability in semi-arid watersheds. Monitoring Ecological Condition in the Western. Springer, United States, pp. 285–298.
Imran, A.M., 2019. Flood and landslide vulnerability as natural hazard in parepare City. In: IOP Conference Series: Earth and Environmental Science. IOP Publishing. pp. 12079.
Krause, P., Boyle, D.P., Bäse, F., 2005. Comparison of different efficiency criteria for hydrological model assessment. Adv. Geosci. 5, 89–97.
Lory, J.A., 2018. Agricultural Phosphorus and Water Quality. University of Missouri-Columbia.
Lu, D., Weng, Q., 2007. A survey of image classification methods and techniques for improving classification performance. Int. J. Remote Sens. 28, 823–870.
Masek, J.G., Vermote, E.F., Saleous, N.E., Wolfe, R., Hall, F.G., Huemmrich, K.F., Gao, F., Kutler, J., Lim, T.-K., 2006. A Landsat surface reflectance dataset for North America, 1990-2000. IEEE Geosci. Remote Sens. Lett. 3, 68–72. https://doi.org/10.1109/LGRS.2005.857030.
Masek, J.G., Vermote, E.F., Saleous, N., Wolfe, R., Hall, F.G., Huemmrich, K.F., Gao, F., Kutler, J., Lim, T.K., 2012. LEDAPS Landsat calibration, reflectance, atmospheric correction preprocessing code. ORNL DAAC.
Melgani, F., Bruzzone, L., 2004. Classification of hyperspectral remote sensing images with support vector machines. IEEE Trans. Geosci. Remote Sens. 42, 1778–1790.
Moreno, G., Albrecht, A.J.P., Albrecht, L.P., Junior, C.P., Pivetta, L.A., Tessele, A., Lorenzetti, J.B., Furtado, R.C.N., 2018. Application of nitrogen fertilizer in high-demand stages of soybean and its effects on yield perform. Aust. J. Crop Sci. 12, 16.
Moriasi, D.N., Arnold, J.G., Van Liew, M.W., Bingner, R.L., Harmel, R.D., Veith, T.L., 2007. Model evaluation guidelines for systematic quantification of accuracy in watershed simulations. Trans. ASABE 50, 885–900.
Naranjo, R.C., Niswonger, R.G., Smith, D., Rosenberry, D., Chandra, S., 2019. Linkages between hydrology and seasonal variations of nutrients and periphyton in a large oligotrophic subalpine lake. J. Hydrol. 568, 877–890. https://doi.org/10.1016/j.jhydrol.2018.11.033.
Nash, J.E., Sutcliffe, J.V., 1970. River flow forecasting through conceptual models part I—a discussion of principles. J. Hydrol. 10, 282–290.
Neitsch, S.L., Arnold, J.G., Kiniry, J.R.ea1, Srinivasan, R., Williams, J.R., 2002. Soil and water assessment tool user's manual version 2000. GSWRL Rep. 202.
Neitsch, S.L., Arnold, J.G., Kiniry, J.R., Williams, J.R., King, K.W., 2005. Soil and Water Assessment Tool Theoretical Documentation. version 2005. USDA-ARS Grassland. Soil Water Res. Lab., Temple, Tex, pp. 8.
Ni, X., Parajuli, P.B., 2018. Evaluation of the impacts of BMPs and tailwater recovery system on surface and groundwater using satellite imagery and SWAT reservoir function. Agric. Water Manag. 210, 78–87.
Nie, W., Yuan, Y., Kepner, W., Nash, M.S., Jackson, M., Erickson, C., 2011. Assessing impacts of Landuse and Landcover changes on hydrology for the upper San Pedro watershed. J. Hydrol. 407, 105–114. https://doi.org/10.1016/j.jhydrol.2011.07.012.
NOAA NCEI, 2020. National Oceanic and Atmospheric Administration, National Centers for Environmental Information. [WWW Document]. URL. https://www.ncdc.noaa.gov/.
NRCS, 2020. United States Department of Agriculture, Natural Resource Conservation Service. [WWW Document]. URL. https://www.nrcs.usda.gov/wps/portal/nrcs/site/national/home/.
Parajuli, P.B., Jayakody, P., Sassenrath, G.F., Ouyang, Y., Pote, J.W., 2013. Assessing the impacts of crop-rotation and tillage on crop yields and sediment yield using a modeling approach. Agric. Water Manag. 119, 32–42.
Parajuli, P.B., Jayakody, P., Sassenrath, G.F., Ouyang, Y., 2016. Assessing the impacts of climate change and tillage practices on stream flow, crop and sediment yields from the Mississippi River Basin. Agric. Water Manag. 168, 112–124. https://doi.org/10.1016/j.agwat.2016.02.005.
Patel, N.N., Angiuli, E., Gamba, P., Gaughan, A., Lisini, G., Stevens, F.R., Tatem, A.J., Trianni, G., 2015. Multitemporal settlement and population mapping from Landsat using Google Earth Engine. Int. J. Appl. Earth Obs. Geoinf. 35, 199–208.
Peddi, D., Kumar, K., 2019. Farmer's Perception on Soil Erosion in Rainfed Watershed Areas of Telangana, India.
Peng, W., Li, S., He, Z., Ning, S., Liu, Y., Su, Z., 2019. Random Forest classification of rice planting Area using multi-temporal polarimetric radarsat-2 data. IGARSS 2019-2019 IEEE International Geoscience and Remote Sensing Symposium. IEEE, pp. 2411–2414.
Pokhrel, B., 2018. Impact of Land Use Change on Flow and Sediment Yields in the Khokana Outlet of the Bagmati River, Kathmandu, Nepal. Hydrology 5, 22.
Qi, J., Zhang, X., Yang, Q., Srinivasan, R., Arnold, J.G., Li, J., Waldholf, S.T., Cole, J., 2020. SWAT ungauged: water quality modeling in the Upper Mississippi River Basin. J. Hydrol. 584, 124601. https://doi.org/10.1016/j.jhydrol.2020.124601.
Raeisi-Vanani, H., Soltani-Toudeshki, A.R., Shayannejad, M., Ostad-Ali-Askari, K., Ramesh, A., Singh, V.P., Eslamian, S., 2017. Wastewater and magnetized wastewater effects on soil erosion in furrow irrigation. Int. J. Res. Stud. Agric. Sci. 3, 1–14.
Reddy, D.D., Rao, A.S., Takkar, P.N., 1999. Effects of repeated manure and fertilizer phosphorus additions on soil phosphorus dynamics under a soybean-wheat rotation. Biol. Fertil. Soils 28, 150–155.
Risal, A., Parajuli, P.B., 2019. Quantification and simulation of nutrient sources at watershed scale in Mississippi. Sci. Total Environ. 670, 633–643.
Ritchie, M., Debba, P., Lück-Vogel, M., Goodall, V., 2018. Assessment of accuracy: systematic reduction of training points for maximum likelihood classification and mixture discriminant analysis (Gaussian and t-distribution). South African J. Geomatics 7, 132–146.
Rosenfield, G.H., Fitzpatrick-Lins, K., 1986. A coefficient of agreement as a measure of thematic classification accuracy. Photogramm. Eng. Remote Sensing 52, 223–227.
Rwanga, S.S., Ndambuki, J.M., 2017. Accuracy assessment of land use/land cover classification using remote sensing and GIS. Int. J. Geosci 8, 611–622.
Shah, H.L., Zhou, T., Huang, M., Mishra, V., 2019. Strong influence of irrigation on water budget and land surface temperature in indian subcontinental river basins. J. Geophys. Res. Atmos. 124, 1449–1462.
Sharpley, A.N., Syers, J.K., 1979. Phosphorus inputs into a stream draining an agricultural watershed. Water Air Soil Pollut. 11, 417–428.
Smits, P.C., Dellepiane, S.G., Schowengerdt, R.A., 1999. Quality assessment of image classification algorithms for land-cover mapping: a review and a proposal for a cost-based approach. Int. J. Remote Sens. 20, 1461–1486. https://doi.org/10.1080/014311699212560.
Snipes, C.E., Nichols, S.P., Poston, D.H., Walker, T.W., Evans, L.P., Robinson, H.R., 2005. Current agricultural practices of the Mississippi Delta mississippi. Agric. For. Exp. Station. Bull. 1143.
USGS, 2020. United States Geological Survey. [WWW Document]. URL. https://www.usgs.gov/.
USGS Landsat Missions, 2020. United States Geological Survey, Landsat Science Product. [WWW Document]. URL. https://www.usgs.gov/land-resources/nli/landsat/landsat-science-products?qt-science_support_page_related_con=2#qt-science_support_page_related_con.
Vermote, E., Justice, C., Claverie, M., Franch, B., 2016. Preliminary analysis of the performance of the Landsat 8/OLI land surface reflectance product. Remote Sens. Environ. 185, 46–56. https://doi.org/10.1016/j.rse.2016.04.008.
Welch, A.P., 2019. The Composition and Distribution of Stream Restoration Activity: An Analysis of Implementation at Multiple Scales. The Pennsylvania State University.
Zhao, L., Hou, R., Wu, F., 2018. Effect of tillage on soil erosion before and after rill development. L. Degrad. Dev. 29, 2506–2513. https://doi.org/10.1002/ldr.2996.